JACS
JOURNAL OF THE AMERICAN CHEMICAL SOCIETY
Article
pubs.acs.org/JACS

The Ligand Shell as an Energy Barrier in Surface Reactions on Transition Metal Nanoparticles

Jeremy G. Smith[†] and Prashant K. Jain*[,†,‡,§]

[†]Department of Chemistry, University of Illinois, Urbana−Champaign, Illinois 61801 United States
[‡]Department of Physics, University of Illinois, Urbana−Champaign, Illinois 61801 United States
[§]Materials Research Lab, University of Illinois, Urbana−Champaign, Illinois 61801 United States

Supporting Information

ABSTRACT: Transition metal nanoparticles, including those employed in catalytic, electrocatalytic, and photocatalytic conversions, have surfaces that are typically coated with a layer of short or long-chain ligands. There is little systematic understanding of how much this ligand layer affects the reactivity of the underlying surface. We show for Ag nanoparticles that a surface-adsorbed thiol layer greatly impedes the kinetics of an ionic chemical reaction taking place on the Ag surface. The model reaction studied is the galvanic exchange of Ag with Au^{3+} ions, the kinetics of which is measured on individual thiol-coated nanoparticles using in situ optical scattering spectroscopy. We observe a systematic lowering of the reactivity of the nanoparticle as the chain length of the thiol is increased, from which we deduce that the ligand layer serves as an energy barrier to the transport of incoming/outgoing reactive ions. This barrier effect can be decreased by light irradiation, resulting from weakened binding of the thiol layer to the metal surface. We find that the influence of the surface ligand layer on reactivity is much stronger than factors such as nanoparticle size, shape, or crystallinity. These findings provide improved understanding of the role of ligand or adsorbates in colloidal catalysis and photocatalysis and have important implications for the transport of reactants and ions to surfaces and for engineering the reactivity of nanoparticles using surface passivation.

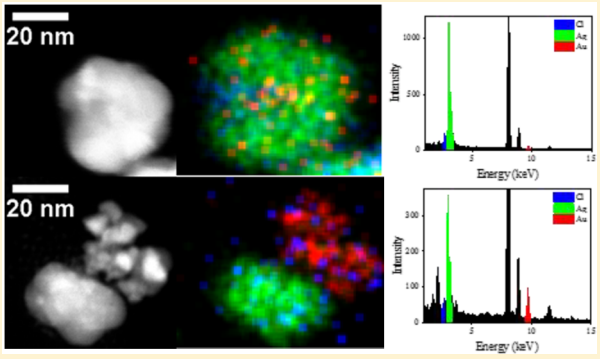

INTRODUCTION

The ligand shell is ubiquitous in colloidal nanoscience. The surfaces of inorganic nanoparticles are typically covered with a shell of organic ligands. These ligands serve the critical role of stabilizing nanoparticles in the colloidal state by enhancing solvation and sterically hindering internanoparticle coalescence.[1] Other functions such as electronic passivation of less-coordinated surface atoms are also known.[2−4] However, the ligand layer can play an inadvertent role in applications where access to the inorganic nanoparticle surface is desirable, for instance, when ligand-coated nanoparticles are used as colloidal catalysts, photocatalysts, in batteries or electrochemical cells. For instance, Talapin and co-workers have shown that long-chain hydrocarbon-based ligands serve as insulating barriers to electron transport in assembled films of closely packed ligand-passivated CdSe nanocrystals.[5]

Ligands play an important role in modulating the reactivity of metal centers, a fact that has long been appreciated in inorganic chemistry. In the synthetic colloidal nanocrystal community, the role of ligands in modulating the growth of shape-controlled nanoparticles is central.[6,7] How surface reactivity is affected by the ligand shell, a common topic of investigation in the surface science community,[8−12] is however only beginning to be elucidated in the nanoparticle community. Herein, we ask how the ligand shell influences a common nanoscale transformation, that of galvanic exchange. The specific system studied is the galvanic exchange of Ag nanoparticles capped with organic thiols by Au ions.[13,14] In this system, Au^{3+} ions from solution diffuse to the Ag nanoparticle surface and undergo reduction to form Au, which gets deposited on the surface. Concomitantly, as required by electrochemical balance, Ag atoms from the nanoparticle are oxidized to Ag^{+} ions, which diffuse into the solution. Galvanic exchange has become an important method for engineering nanostructures of a variety of metals,[15,16] metal oxides,[17] and semiconductors,[18] and is beginning to find applications in medicine,[19] catalysis,[20] and sensing.[21]

It has been observed that the nature of the passivating ligand influences the final morphology of the nanostructure formed from galvanic exchange.[22] What is the precise mechanistic origin of this effect? In addition to modification of surface energies, the ligand layer can be expected to hinder diffusion of electrons, ions, adsorbates, or reactive molecules to the surface of the nanoparticle. What role does transport across the organic ligand interface play in the overall reactivity of the nanoparticle? The latter questions motivate our study, wherein mechanistic conclusions are made on the basis of ensemble-free reaction

Received: January 13, 2016
Published: May 6, 2016

DOI: 10.1021/jacs.6b00179
J. Am. Chem. Soc. 2016, 138, 6765−6773

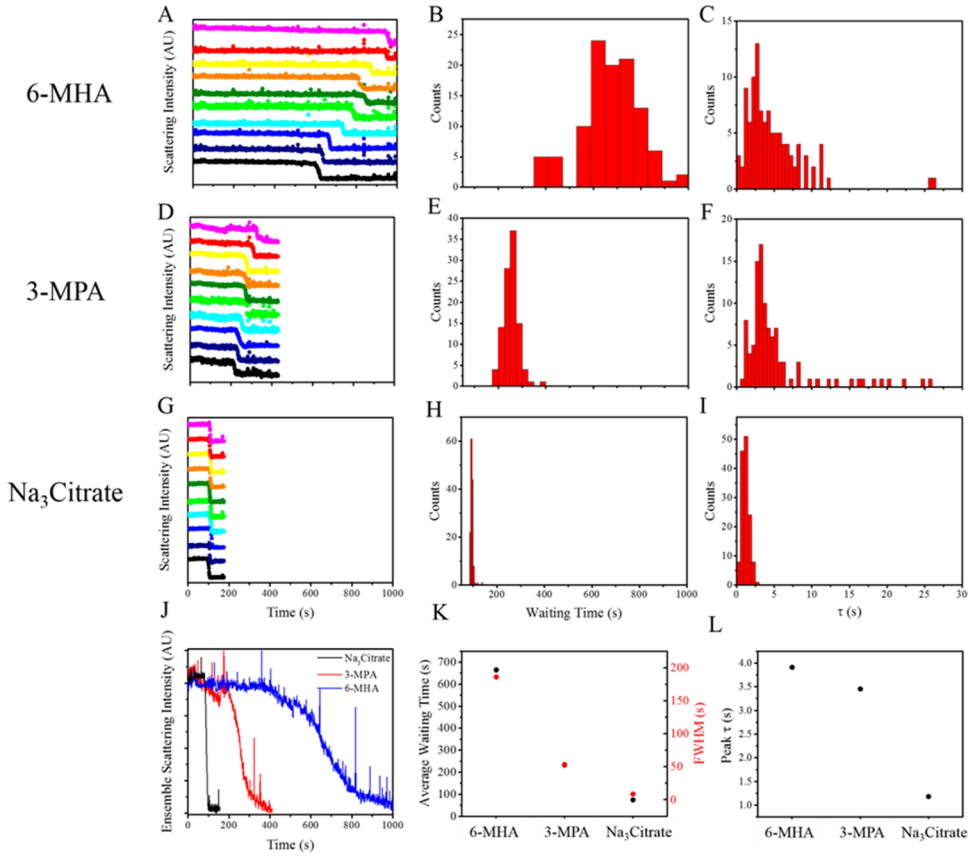

Figure 1. Kinetics of the galvanic exchange of Ag nanoparticles for different ligand coatings. Representative single-nanoparticle reaction trajectories (A,D,G), waiting-time distributions (B,E,H) and τ distributions (C,F,I) for 34 nm Ag nanospheres coated with 6-MHA (A,B,C), 3-MPA (D,E,F), and Na_3Citrate (G,H,I) undergoing galvanic replacement with Au(III)Cl_3 in DI water. Entry of the Au(III)Cl_3 solution into the flow cell occurred at $t = 0$ s. All experiments were performed with a Au(III)Cl_3 concentration of 6 μM, a flow rate of 1.5 mL/h, and 12.11% of maximum lamp power. The ensemble trajectory, generated by averaging all single-nanoparticle trajectories, is shown for each of the three ligand coatings (J). Average waiting time (K, black dots), fwhm of the waiting time distribution (K, red dots) and peak τ (L) are shown as a function of the type of ligand coating. Data from 138, 104, and 107 nanoparticles was used to generate the ensemble trajectory and distributions for the Na_3Citrate, 3-MPA, and 6-MHA cases, respectively.

kinetics measured *in situ* on single nanoparticles. Particularly, instructive in the model galvanic exchange reaction is the influence of the ligand shell thickness on reactive ion transport, akin to studies on electron transfer across insulating organic monolayers.[23,24] By variation of the chain length of the hydrocarbon backbone of the thiol, it was possible to vary the thickness of the ligand coating and study the resulting effect on the kinetics of the galvanic exchange reaction. We found that the presence of a surface-bound thiol monolayer greatly impeded reaction rates, without altering the fundamental nature of the transformation, an effect that becomes stronger with increasing chain length of the thiol. The thickness effect suggests that the ligand shell serves as an energy barrier to the diffusion of ions to/from the nanoparticle surface. From a detailed study of various parameters, the influence of the ligand shell on reactivity is found to be much stronger than the effect of size, shape, or crystallinity of the nanoparticles. We also find that the barrier effect can be decreased by light irradiation, wherein the binding of the ligand layer to the surface is weakened. In addition to the fundamental insights into interfacial chemistry and transport phenomena, one implication of these results for catalysis/photocatalysis is that metal nanoparticle reactivity can be tuned by a combination of ligand passivation and light irradiation

METHODS

For the measurement of reaction kinetics, we monitored the galvanic exchange reaction on individual Ag nanospheres using in situ dark-field scattering spectroscopy (see detailed procedure in the SI). Citrate-coated Ag nanospheres were first immobilized within a microfluidic flow cell and incubated with a solution of a carboxylic acid thiol. The thiols, known to form strong Ag−S bonds, replace the weakly bound citrate ligands at the nanoparticle surface. Close to saturation coverage of the thiol can be achieved after 15 min of incubation as evidenced by the results of a separate study.[25] The thiol-coated nanospheres were then subject to galvanic exchange with a Au(III)Cl_3 solution. The area-density of immobilized nanoparticles was maintained low enough such that, on average, individual nanoparticles were separated by distances greater than the diffraction limit, thereby enabling single-nanoparticle resolution. Due to the strong localized surface plasmon resonance (LSPR) of the 34 nm Ag nanospheres, their scattering cross-section is large enough to allow single-nanoparticle-level sensitivity in dark-field scattering.[26−30] Upon exposure to a sufficient concentration of Au(III)Cl_3, Ag from a nanosphere is dissolved in the form of Ag^+ (or precipitated in the form of AgCl) and Au is concomitantly deposited on the nanospherical template.[31] Due to the presence of strong d → sp transitions in the blue region of the electronic spectrum of Au, the LSPR of the final Au-containing nanostructure is damped relative to that of the starting Ag nanosphere. Therefore, in the course of galvanic exchange, there is a decrease in the scattering intensity (Movies S1−S3), which can be monitored in real-time to generate a single-nanoparticle reaction trajectory. Note that AgCl deposition,

DOI: 10.1021/jacs.6b00179
J. Am. Chem. Soc. 2016, 138, 6765−6773

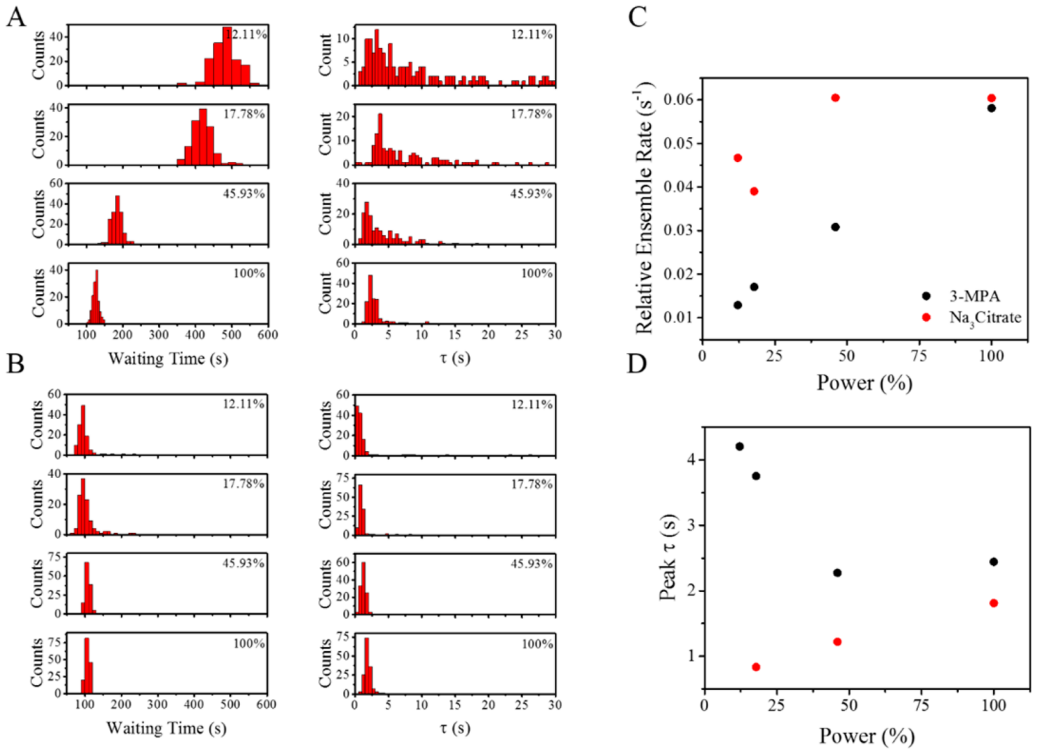

Figure 2. Effect of light on kinetics of galvanic exchange of ligand-coated nanoparticles. For a range of lamp illumination powers, the waiting time distribution (left) and τ distribution (right) for 34 nm Ag nanospheres coated with 3-MPA (A) and Na_3Citrate (B) are shown. All experiments were performed at a Au(III)Cl_3 concentration of 5 μM and a flow rate of 1.5 mL/h. The relative lamp power is shown as a % of the maximum. Relative ensemble reaction rate (C) and single-nanoparticle peak τ (D) are shown as a function of lamp power (%) for 3-MPA and Na_3Citrate coated nanoparticles. Relative ensemble rate is defined as the inverse of the fwhm of the waiting time distribution. Ensemble rates of the 3-MPA-coated nanoparticles show strong power dependence unlike Na_3Citrate coated nanoparticles. Peak τ decreases with increasing lamp power for 3-MPA-coated nanoparticles. Note that the data point at the lowest power for the Na_3Citrate functionalized particles is not shown since the acquisition time in this experiment (2 s) was too large to accurately determine τ. Power dependence of the kinetics for 6-MHA and 11-MUA coated nanoparticles is shown in Figure S6.

while prevalent to a small extent in this galvanic exchange reaction, does not cause a significant damping of the scattering intensity, as compared to the effect of galvanic displacement of Ag by Au.

Single-nanoparticle trajectories (Figure 1A,D,G) give us information about the dynamics of galvanic exchange, which is otherwise smeared out in an ensemble-averaged trajectory (Figure 1J).[32−44] From single-nanoparticle intensity trajectories, we observe that each individual nanoparticle, following a waiting period, makes a rather abrupt switch from an Ag nanosphere (high scattering intensity state) to the final exchanged nanostructure (low scattering intensity state). The instant of onset of this transition, given by the waiting time, varies from one nanoparticle to another (most evident in Figure 1A). The waiting times are stochastically distributed over the nanoparticle population and appear to follow a Gaussian distribution (Figure 1B,E,H). From a fit to the Gaussian function (examples shown in Figure S2), one can obtain both an average waiting time and the spread in waiting times in the form of a full-width-at-half-maximum (fwhm). Both the average waiting time and the fwhm are inversely related to the rate of progress of the galvanic exchange averaged over the nanoparticle population.

In the past,[39] we have shown (as subsequently confirmed by others[45]) that the behavior observed in single-nanoparticle trajectories is a result of a two-step mechanism:

(i) There is a precursor step in the galvanic transformation of the nanoparticle, which involves the stochastic nucleation of a void (collection of Ag vacancies) on the surface of the Ag nanoparticle. The waiting time signifies the period before a void larger than a critical size is nucleated in the nanoparticle.

(ii) Following the formation of a critical void in a nanoparticle, rapid galvanic exchange takes place across the bulk of the nanoparticle, limited only by the mass transport of depositing Au^{3+} ions and/or dissolving Ag^{+} ions. The time it takes for this mass-transport-limited transformation is signified by a time constant (τ), obtained by fitting the single-nanoparticle trajectory to a Boltzmann-like sigmoid function, as shown in Figure S1. Since there is small spread in τ values over the nanoparticle population possibly due to structural/morphological/surface differences, we refer to the peak τ of the distribution, obtained by log-normal fitting of this tailed distribution (examples shown in Figure S2).

Under typical conditions, τ is smaller than the average waiting time or the fwhm, implying that void nucleation is the rate-limiting step in the reaction. The nucleation of a critical void requires the reduction of multiple Au^{3+} ions, as reflected in a nonlinear reaction order with respect to the Au^{3+} concentration. Under conditions, such as a higher Au^{3+} concentration, void nucleation takes place at a higher rate, the waiting times shift to a lower average, the spread of waiting times becomes narrower (smaller fwhm) and the galvanic exchange is seen to proceed faster at the ensemble level.

RESULTS AND DISCUSSION

Effect of Ligand Length on Reaction Rate. Using information (fwhm, average waiting time, peak τ) from a large set of such single-nanoparticle trajectories, we were able to determine the effect of the ligand shell separately on the kinetics of the two elementary steps of the transformation: void nucleation and subsequent mass-transport limited dissolution of Ag and deposition of Au. We compared the behavior of Ag nanospheres coated with Na_3Citrate with those coated with carboxylic acid-terminated thiols of three different chain

DOI: 10.1021/jacs.6b00179
J. Am. Chem. Soc. 2016, 138, 6765−6773

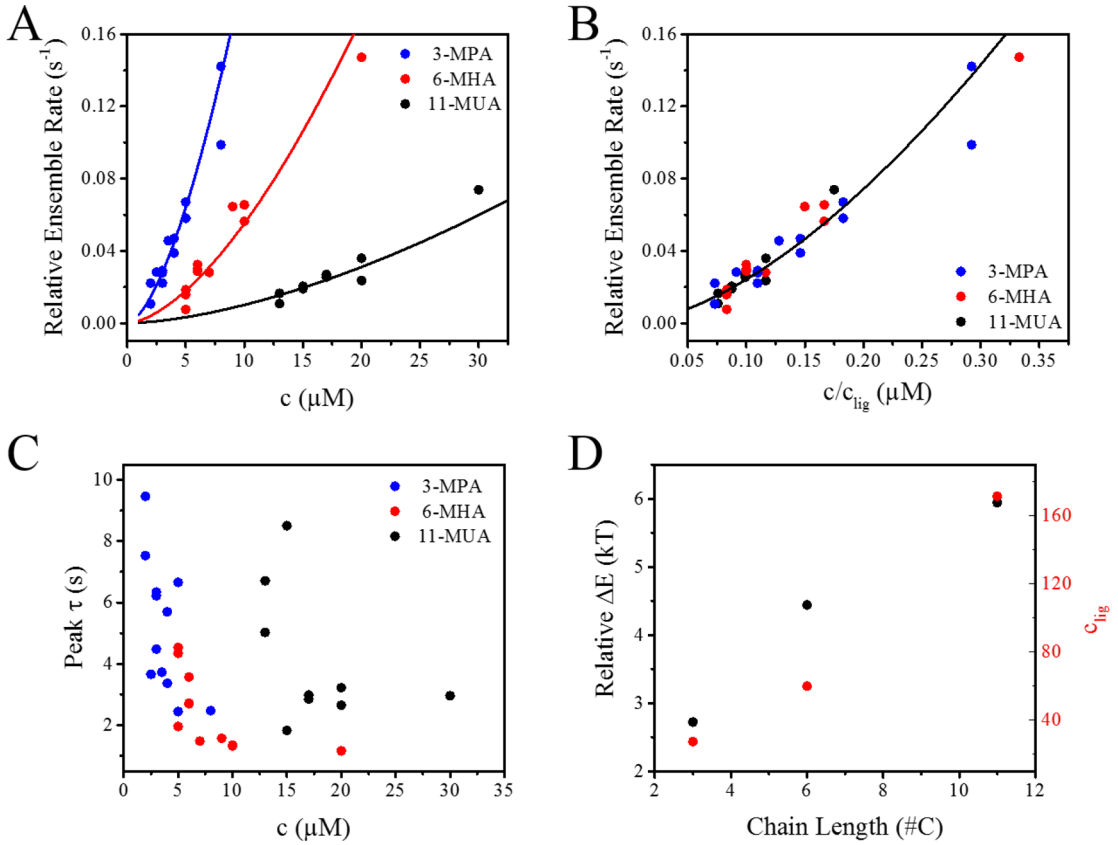

Figure 3. Effect of chain length of carboxylic acid thiols on kinetics of galvanic exchange. Relative ensemble rate (A) and single nanoparticle peak τ (C) as a function of Au(III)Cl_3 concentration for 34 nm Ag nanospheres coated with 3-MPA (blue), 6-MHA (red) and 11-MUA (black). All experiments were performed in DI water at a flow rate of 1.5 mL/h and at 100% of maximum lamp power. In A, fits to rel rate = $a(c/c_{lig})^b$ are shown as solid lines, with a global R^2 value of 0.86. Ensemble rate as a function of the scaled concentration c/c_{lig} is shown in combined manner for all three coatings in (B). c_{lig} and relative barrier height, ΔE, are shown in units of kT as a function of chain length in # of carbon atoms (D). The histograms used to generate data in this figure are shown in Figures S8−S10.

lengths: 3-mercaptopropionic acid (3-MPA), 6-mercaptohexanoic acid (6-MHA), and 11-mercaptoundecanoic acid (11-MUA). The procedure of surface coating is described in the SI. Results of galvanic exchange on surface functionalized nanoparticles are presented in Figure 1.

Whereas thiols form a well-bound layer on the nanoparticle surface, Na_3Citrate is known to form a weakly adsorbed ligand layer with possibly sparser equilibrium coverage.[46−48] Exchange dynamics are similar: abrupt switch-like transformation of individual nanoparticles is seen for both thiol and Na_3Citrate cases. However, the reaction kinetics are markedly different for the thiol vs the Na_3Citrate cases at the same Au^{3+} concentration. Compared to the Na_3Citrate, the ensemble conversion progresses much more slowly in the case of the thiols (Figure 1J). The waiting time is shifted to a significantly higher average and the fwhm of the waiting time distribution is also significantly higher (Figure 1K). The latter suggests that whereas the Na_3Citrate is easily displaced from the nanoparticle surface to facilitate initial exchange events, the presence of the strongly bound thiol coating is an impediment to the nucleation of a void on the nanoparticle surface, the critical step in the transformation. It is possible that thiol passivation renders surface Ag atoms more stable against dissolution. However, there is an observable effect of the carbon chain length of the alkanethiol, which suggests phenomena other than surface energies are at play, as will be discussed later. The slowing down in the ensemble reaction is much more pronounced for the longer-chain 6-MHA than for the shorter-chain 3-MPA, under identical conditions (Figure 1). The average waiting time and fwhm are higher for the former. Furthermore, for Ag nanoparticles capped with an 11-MUA layer, the impeding effect is so dramatic, that no exchange is seen in this case even after 2000 s of exposure under identical reaction conditions (Movie S4).

In addition to hindered nucleation, mass-transport of ions (postnucleation) also appears to be impeded in the presence of the hydrophobic thiol coating, as seen from a comparison of time constants for single-nanoparticle transformation, τ. It appears from the peak τ values (Figure 1K) that it takes 3−4 times longer for a thiol-coated nanoparticle to transform as compared to a Na_3Citrate-coated nanoparticle. There, however, appears to be little effect of the carbon chain length on τ (Figure 1L).

Influence of Light Irradiation on Ligand Effect. We were also able to decrease this "blocking" effect of the ligand shell by means of light excitation. Visible light excitation of thiol-coated nanoparticles is known to result in the desorption of thiols from the nanoparticle surface,[49] either due to photothermal heating,[50] thiol photooxidation,[51] or due to photoinduced energy transfer into Au−S bonds.[46] Figure 2 shows the effect of light irradiation on the galvanic exchange of 3-MPA coated Ag nanoparticles. With an increase in the light irradiation power, an increase in the ensemble rate of exchange was seen. The average waiting time and fwhm systematically

DOI: 10.1021/jacs.6b00179
J. Am. Chem. Soc. 2016, 138, 6765−6773

decreased with an increase in the light irradiation power (Figure 2A, left) and the peak τ decreased (Figure 2A, right). Experiments performed with 6-MHA and 11-MUA coated nanoparticles showed a similar photoeffect (Figure S6). At the highest power tested, kinetic parameters approached those of Na_3Citrate capped nanoparticles. These results indicate that the passivating thiol shell on the nanoparticle surface is disrupted (eq 1), due to light excitation:

$$\mathrm{Ag{-}SR} \overset{h\nu}{\rightleftharpoons} \mathrm{Ag_{bare}} + {-}\mathrm{SR_{physisorbed}} \quad (1)$$

Higher the excitation power, greater is the likelihood of a nanoparticle presenting a defective ligand shell with its surface partially exposed to the Au^{3+} solution, such that in the limiting case, void nucleation and ionic transport become as facile as in the case of uncoated or Na_3Citrate-capped nanoparticles. In the case of weakly bound Na_3Citrate, which is easily displaced even in the absence of light, the photoeffect is weak (Figure 2B). It is worth noting that similar photoinduced ligand displacement has been observed on semiconductor nanocrystals.[52−54] In these cases, the desorption of thiols involves their photoxidation to disulfides, induced by electron injection into oxygen present in solution. Since oxygen is present in our solution (as expected from its solubility of 8 mg/mL in DI water at room temperature and pressure), it is plausible that a similar mechanism is at play here. However, selective energy deposition into Ag−S bonds either by photothermal means or via hot electron transfer (chemical interface damping) cannot be ruled out. Determination of the precise mechanism of the visible light-induced thiol desorption, while outside the scope of the current study, is worthy of future investigations.

Au^{3+} Concentration Dependence of Reaction Rate. It has been shown[39] that the nucleation of a critical sized void on the Ag nanoparticle surface requires multiple Au^{3+} ions to be reduced to Au(0) at the Ag surface; concomitantly multiple Ag atoms undergo oxidative dissolution. The reaction kinetics therefore shows a nonlinear reaction order with respect to the concentration of $Au(III)Cl_3$. From the dependence of the reaction rate on the $Au(III)Cl_3$ concentration for coatings of different carbon chain lengths (Figure 3 and Figures S7−10), we obtain further insights into the mechanistic role of the ligand coating. For all coatings, the relative ensemble rate (which is simply given by 1/fwhm as established by us in the past[39]), increases with an increase in the $Au(III)Cl_3$ concentration, c (Figure 3A).

It must be noted that, as a result of the nonlinear concentration dependence of kinetics for the galvanic exchange system,[39] small variations in the reaction conditions can produce significant fluctuations in the reaction rate. In fact, Figure 3 contains at least two trials at each concentration. The measured rate can differ by up to 2-fold between trials, particularly, at the lowest concentration. The discrepancy between experimental trials likely originates from unavoidable variations in the underlying substrate (hydroxylated SiO_2) to which the metal nanoparticles are affixed. Despite our best attempts to rigorously clean the substrates, we believe that there are always variations in the local pH, glass surface structure, and/or trace contaminant levels that can affect kinetics. As well documented in the single molecule biophysics community, there is an open need for exceptionally reliable methods to prepare reliably uniform substrates.[55] Despite the observed heterogeneity, the rate always varied systematically with concentration for a given set of trials. Furthermore, there was always good agreement between the average waiting time and the fwhm across all trials (Figure S7, correlation coefficient of 0.84). Third, in all of the trials, a longer chain ligand exhibited a smaller ensemble rate than all of the trials performed with a shorter one at the same concentration. In other words, the fluctuations were not large enough to occlude the systematic dependence on ligand chain length, discussed below.

Scaling of Concentration Dependence between Different Ligand Lengths. When the ensemble reaction is plotted vs $Au(III)Cl_3$ concentration, a trend is found for each ligand length (Figure 3A). The longer ligand shows a lower rate at the same $Au(III)Cl_3$ concentration. However, data points for the three ligand lengths follow the same curve if we plot the rate vs a scaled concentration c/c_{lig} instead of c:

$$\text{rel rate} = a\left(\frac{c}{c_{lig}}\right)^{b} \quad (2)$$

where c_{lig} is a ligand length-dependent unit-less scaling factor. Here, a is a proportionality factor of 1 M^{-b} s^{-1} for consistency of units and b found from fitting to be ∼2 for all ligand lengths signifies the nonlinear reaction order.

Model of Ligand Length-Dependent Barrier Effect. The observed scaling behavior of reaction rate vs c/c_{lig} implies the following. The galvanic exchange reaction rate is not dictated by the bulk Au^{3+} concentration c, but it is dictated by some effective Au^{3+} concentration at the Ag nanoparticle surface. The insulating, hydrophobic ligand shell acts as an energy barrier against the transport of Au^{3+} ions from the bulk to the nanoparticle surface. Due to this hindered transport of Au^{3+}, the surface Au^{3+} concentration (or chemical potential) is lower than the bulk concentration. If the fraction of Au^{3+} ions that can transfer across the ligand barrier and reach the surface is denoted by $1/c_{lig}$, then the effective, steady-state surface concentration is simply c/c_{lig}. One may hypothesize that longer the ligand, greater the barrier effect, smaller this transported fraction $1/c_{lig}$, and lower the effective surface concentration c/c_{lig}. This is indeed what we find from the values of c_{lig} extracted from fitting the rate data to eq 2 (Figure 3D). From, the value of c_{lig}, we can also estimate the relative barrier height, rel ΔE, for each ligand length. This is because the fraction of ions that is transferred across the ligand barrier, $1/c_{lig}$, is given by $\exp(-\text{rel } \Delta E/kT)$. Thus:

$$\exp(-\text{rel } \Delta E/kT) = 1/c_0 \quad (3)$$

$$\text{rel } \Delta E = kT \ln c_0 \quad (4)$$

This ligand length-dependence of ionic transport appears analogous to the distance dependence of the rate of electron transfer across insulating barriers.[56−58] There is another interesting point to be made from our results in the 11-MUA case, where no exchange is seen even at the highest Au^{3+} concentrations employed in the single-nanoparticle experiments. Possibly, for this long chain length, the energy barrier is so high that the steady state Au^{3+} concentration at the surface is not sufficient enough to nucleate large-enough voids and initiate galvanic exchange. It is also worth mentioning an alternate explanation for the ligand length-dependent kinetics, which is difficult to resolve from the barrier thickness effect proposed above. Longer thiols are known to form self-assembled monolayers that are more thermodynamically stable.[59] The lower prevalence of dynamically formed defects

DOI: 10.1021/jacs.6b00179
J. Am. Chem. Soc. 2016, 138, 6765−6773

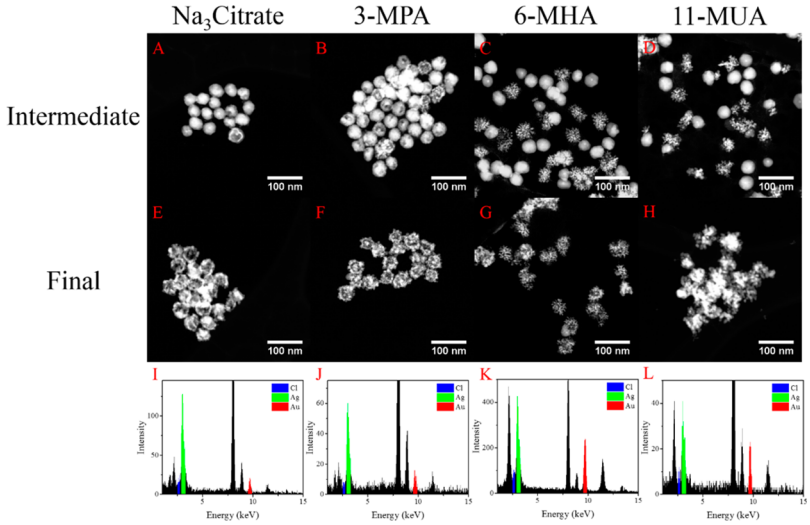

Figure 4. Ligand coating on nanoparticle impacts the morphology of the final nanostructure. High-angle annular dark-field STEM images (top and middle rows) and wide-field EDS spectra (bottom row) of nanostructures obtained from galvanic exchange of 34 nm Ag nanoparticles coated with a shell of Na_3Citrate (A,E,I), 3-MPA (B,F,J), 6-MHA (C,G,K) and 11-MUA (D,H,L) respectively. Galvanic exchange was performed on a bulk colloidal suspension of Ag nanospheres in a cuvette by titration against a Au(III)Cl_3 solution. The extent of the exchange was monitored by UV−vis spectrophotometry (Figure S11). HAADF-STEM images at intermediate conversion (top row) showed distribution of morphologies ranging from unexchanged to fully exchanged. EDS spectra of the fully exchanged samples (bottom row) show that the relative Au content in the final nanostructures depends on the ligand coating, with Ag/Au atomic ratios of 6.6, 3.6, 1.4, and 1.7 for Na_3Citrate, 3-MPA, 6-MHA, and 11-MUA coated nanoparticles, respectively.

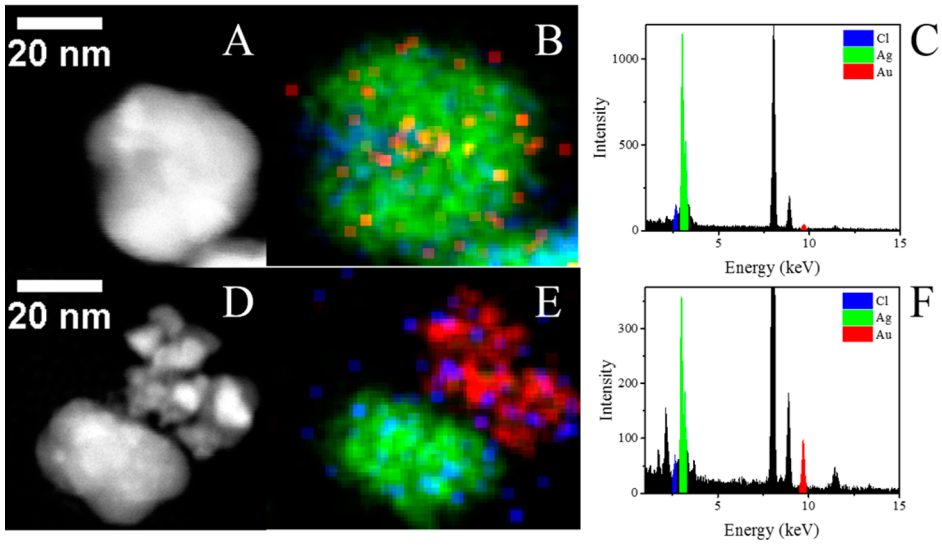

Figure 5. Short versus long ligand cases show remarkably different nanostructure morphology and composition profile. (A,D) HAADF-STEM images, (B,E) EDS maps, and (C,F) EDS spectra for a representative nanostructure at the intermediates stage of galvanic exchange of 34 nm Ag nanospheres coated with Na_3Citrate (A,B,C) and 11-MUA (D,E,F). Au is shown in red, Ag in green, and Cl in blue, in maps and spectra. The representative nanostructures were selected from the same samples as those imaged in Figure 4A and D, with corresponding UV−vis spectra shown by red curves in Figure S11 A and D. In the Na_3Citrate case, Au deposition appears to have taken place uniformly over the initial Ag nanoparticle template, whereas in the 11-MUA case, multiple deposited Au regions, completely segregated from the Ag nanoparticle, are seen. From EDS spectra, Ag/Au atomic ratios are found to be 99.9 and 18.6 for the Na_3Citrate and 11-MUA case, respectively.

in the longer chain ligand coating may be the cause of the slower kinetics of ion transport across the shell.

Effect of Ligand Shell on Single Nanoparticle Rates. A similar scaling behavior is also seen in the single nanoparticle τ values (Figure 3C). As shown in the past, τ, which represents the time scale of mass-transport limited exchange, is typically independent of the Au(III)Cl_3 concentration above a threshold concentration. However, below this concentration, it begins to sharply increase, indicating a regime where the rate of atomistic exchange events becomes limited by the availability of Au^{3+} at the nanoparticle surface. This threshold concentration (ca. 5 μM for 3-MPA, ca. 10 μM for 6-MHA, and ca. 15 μM for 11-MUA) appears to be larger for longer chain ligands. This finding (and that in Figure 1L) is consistent with the role of the ligand shell as a barrier to the transport of Au^{3+} ions to the nanoparticle surface.

Influence of Ligand Shell on Final Nanostructure Morphology. Furthermore, in addition to the kinetics, we found that the nature of the ligand coating influenced the structure/morphology of the nanostructures produced by

DOI: 10.1021/jacs.6b00179
J. Am. Chem. Soc. 2016, 138, 6765−6773

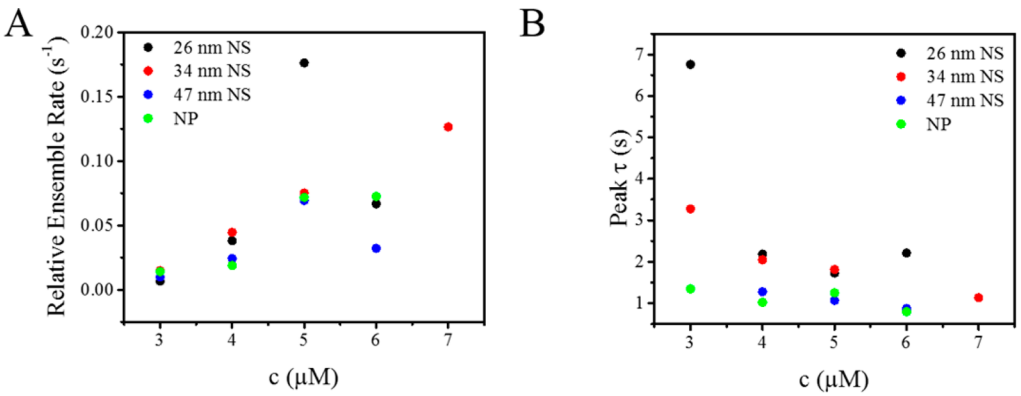

Figure 6. Factors such as size, shape, or crystallinity do not show as strong an effect on reaction kinetics as the nature of the ligand coating. Relative ensemble rate (A) and peak single-nanoparticle τ (B) as a function of Au(III)Cl_3 concentration for Na_3Citrate coated Ag nanospheres of 26, 34, and 47 nm diameters, as well as Ag nanoplates. All experiments were performed at a flow rate of 1.5 mL/h and maximum lamp power, except for the 47 nm nanosphere sample, for which 66% of the maximum power was used.

galvanic exchange (Figure 4, Figure S12). Scanning transmission electron microscopy (STEM) imaging and elemental analysis were performed on nanostructure samples obtained from galvanic exchange of Ag nanospheres in bulk colloidal suspensions, at room temperature, in the absence of light irradiation. In addition to the final product, we also characterized the nanostructures in an intermediate/partial state of exchange (Figures 4 and 5), by limiting the amount of Au^{3+} added and monitoring the progress by UV−vis spectrophotometry (Figure S11). In an irreversible process like galvanic exchange, the concentration of Au(III)Cl_3 added in the titration has correspondence to the exposure time in the kinetics experiment. This correspondence is verified by the fact that the Au(III)Cl_3 concentration required to achieve full conversion in the titration (complete damping of the Ag nanosphere plasmon resonance in UV−vis spectra) followed the same trend (Na_3Citrate < MPA < MHA < MUA) as expected from the ligand length-dependent kinetics. From TEM images at the intermediate state (Figure 4, top row), nanostructures ranged from unreacted to those fully exchanged, with a significant fraction of the nanoparticles partially reacted. We noticed that in order to get to a state where a significant fraction of the nanoparticles had undergone some partial exchange, the thiol-coated nanoparticles needed to be exposed to a much higher Au(III)Cl_3 concentration (see Figure S11) than what was required for the Na_3Citrate-coated nanoparticles. In fact, the trend mirrored the ligand length-dependence of kinetic measurements.

In the case of Na_3Citrate-coated nanoparticles, the final product nanostructure was typically a hollow Au/Ag alloy nanocage (Figures 4E and Figure S12E), templated by the initial Ag nanosphere.[13,14,31,39] 3-MPA coated nanoparticles show a relatively similar final structure to nanoparticles coated with Na_3Citrate (Figures 4F and S12F). However, for 11-MUA-coated nanoparticles, the final nanostructure consisted of a loosely held agglomerate of multiple Au-rich nanodomains of size much smaller than the initial Ag nanosphere (Figures 4H and S12H). The product morphologies in the 6-MHA case were in between the 3-MPA/Na_3Citrate and 11-MUA cases (Figures 4G and S12G), but more similar to the 11-MUA cases, being minimally templated but somewhat alloyed. The relative Au content, of the nanostructures, on average, was found to increase in the order: Na_3Citrate < 3-MPA < 6-MHA ∼ 11-MUA (Figure 4I−L).

Kinetic Origin of Morphology Differences with Different Ligand Coatings. The surface energy of Ag, which is modified by ligand passivation, is an important thermodynamic factor to consider when explaining the observed morphological and compositional differences between the different ligand coatings. However, the fact that the morphological outcome is dissimilar between "chemically" similar coatings (MPA vs MHA vs MUA, all of which involve surface passivation via Ag−S bond formation) prompted us to examine the role played by the length-dependent reaction kinetics for these three ligands.

The observed trend in the product morphology can be explained by the influence of the ligand coating on the nature of atomistic exchange processes (Au deposition and Ag removal) occurring postnucleation. In the case of Na_3Citrate coating, the weakly adsorbed ligand is easily replaced. Therefore, during the spontaneous progress of the exchange reaction postnucleation, Au(0) formed from Au^{3+} reduction is deposited in direct contact with the Ag nanoparticle surface. This close electrochemical contact also allows deposited Au atoms to diffuse into the Ag lattice, in the intermediate stages of exchange, resulting in alloying.[14] A representative example of such an intermediate stage nanostructure is shown in Figure 5A,B. The nature of these processes makes it clear why the initial Ag nanoparticle serves as a structural template for the final hollow nanocage structure (Figure S12A,E). Apart from Au deposition, AgCl can also be formed in the exchange process. However, from the relatively small Cl % measured in EDS spectra of the final nanostructures (Figures 4 and S12), it appears that most of the AgCl is efficiently dissolved and does not affect the ultimate nanostructure morphology under our conditions.

It can be deduced that the loss of templating in the presence of the long-chain thiol ligands, particularly 11-MUA (Figure 5D,E), is a result of reduced electrochemical contact between the Au^{3+} containing-solution and the nanoparticle surface, caused by the thick ligand shell acting as an effective contact barrier. Au^{3+} transport to the nanoparticle surface is significantly hindered in regions where the ligand shell is still intact postnucleation. We propose that despite this, the bulk of the Au^{3+} ions that fail to cross the barrier can competitively reduce to Au(0) on the outer side of the ligand shell, in electrochemical response to Ag atoms oxidatively dissolving from a nucleated void elsewhere on the nanoparticle surface. Despite the lack of direct contact, a redox couple between the two metals is possibly maintained by electron transfer across

DOI: 10.1021/jacs.6b00179
J. Am. Chem. Soc. 2016, 138, 6765−6773

the ligand shell, which can take place much more readily than transport of bulkier ions. As a result of the physicochemical barrier posed by the long-chain ligands, Au, rather than alloying with the Ag lattice, is deposited primarily in the form of discrete nanodomains, as seen from the intermediate stage elemental map (Figure 5E). These phase segregated Au nanodomains are possibly stabilized by a shell of passivating thiols that has undergone slow reorganization. The initial Ag nanosphere, therefore, does not serve as a structural template in the slow exchange reaction with longer chain coatings. The lack of formation of a stable alloy possibly also leads to greater loss of Ag in the course of exchange with longer ligands, explaining the trend in elemental ratios presented in Figures 4 and S12). For the 3-MPA coating, where the short-chain ligand shell poses a relatively weaker barrier, and to a smaller extent for the 6-MHA coating, a significant degree of direct Au deposition/alloying/templating takes place in parallel with some degree of "remote" unstructured Au deposition, thereby explaining the observation of in-between morphologies (Figures 4C,G and S12C,G).

Effect of Nanoparticle Size/Shape versus Ligand Shell on Reaction Kinetics. Finally, we examined the effect of Ag nanoparticle size and shape on the reaction kinetics (Figure 6). The study involved a series of Ag nanospheres of different size (average diameters of 26, 34, and 47 nm) and an additional sample comprising of Ag nanoplates. The 34 and 47 nm nanospheres were entirely polycrystalline, whereas the 26 nm nanospheres were primarily single crystalline. The nanoplates were crystalline, 5 nm thick on average, with their top flat surfaces comprised of the (111) facet of fcc Ag, and containing stacking faults perpendicular to their flat surface. Overall these samples comprise a wide gamut of structural attributes, including differences in nanoparticle volume of >1500%, differences in surface area of >350%, significantly variable defect densities, and significantly different surface sites, including highly under coordinated sites at sharp edges of the prismatic nanoplates. Na_3Citrate was chosen as a ligand to eliminate differences in reaction kinetics originating from the nature of the coating (Figure 1) or light irradiation power (Figure 2). Despite the structural diversity of the nanoparticle samples, there is no dramatic difference in the reaction kinetics. The concentration dependence of ensemble rate follows the same general trend for all these nanoparticle samples of different size and/or morphology (Figure 6A), quite unlike what is seen for different ligand coatings (Figure 3A). While there are some inexplicable differences in single nanoparticle τ values at low concentration, the threshold concentration appears to be similar regardless of size/shape (Figure 6B). Void nucleation at the nanoparticle surface is known to be critical to the progression of the galvanic exchange;[39] therefore, the activity of surface sites is likely to be a crucial determinant of the reaction kinetics. However, it appears that in the case of galvanic exchange studied here, surface reactivity can be manipulated to a much greater extent by means of passivating ligands as compared to handles such as nanoparticle size or shape. Nevertheless, we do not rule out that size may become a much more important factor in reaction kinetics at significantly smaller nanoparticles sizes (ca. few nm), outside the range studied here.

CONCLUSION

Thus, we have shown that the ligand shell has much greater influence on the kinetics of galvanic exchange reactions than factors such as nanoparticle shape, size or internal defect structure. Essentially, the most effective strategy for altering the kinetics of the galvanic exchange reaction and product morphologies is through variation of the ligand coating. Longer chain ligands that are strongly bound to the nanoparticle surface, and/or form well-packed monolayers can act as energy barriers serving to protect the nanoparticle surface from reactions like electrochemical corrosion. Systematic understanding of the effect of ligand passivation on surface reactions and the ability to modify reactivity via photodeprotection has implications beyond galvanic exchange. After all, heterogeneous catalysis and photocatalysis with colloidal nanoparticles are likely to involve effects analogous to those found in this work.

ASSOCIATED CONTENT

Supporting Information

The Supporting Information is available free of charge on the ACS Publications website at DOI: 10.1021/jacs.6b00179.

Reagents and instrumentation; details of flow cell preparation, single-nanoparticle microscopy, single-nanoparticle data processing and analysis, and ensemble solution-phase galvanic exchange experiments for structural characterization; TEM images of Ag nanoparticles of different size/shape used in the study; examples of single-nanoparticle trajectories with fits; examples of fits to waiting time histograms and τ histograms; study showing lack of position bias in waiting times of individual nanoparticles; calibration of lamp power; effect of lamp power on the reactivity of 6-MHA and 11-MUA coated 34 nm nanospheres; average waiting times vs $Au(III)Cl_3$ concentration for 3-MPA, 6-MHA, and 11-MUA cases and for the different size/shape nanoparticles coated with Na_3Citrate; histograms of waiting times and τ values for the entire set of $Au(III)Cl_3$ concentration dependence experiments for Na_3Citrate, 3-MPA, 6-MHA, and 11-MUA cases; UV−vis spectra, representative high-magnification STEM images, EDS maps, and EDS spectra of representative nanostructures obtained from partial galvanic exchange for Na_3Citrate, 3-MPA, 6-MHA, and 11-MUA cases; captions for galvanic exchange microscopy videos. (PDF)

Movie S1. (AVI)

Movie S2. (AVI)

Movie S3. (AVI)

Movie S4. (AVI)

AUTHOR INFORMATION

Corresponding Author

*jain@illinois.edu

Notes

The authors declare no competing financial interest.

ACKNOWLEDGMENTS

The authors acknowledge financial support through an Arnold and Mabel O. Beckman Foundation Young Investigator Award. J.G.S. designed and performed experiments, analyzed results, and wrote the manuscript. P.K.J. conceived studies, designed experiments, analyzed results, and wrote the manuscript.

REFERENCES

(1) Israelachvili, J. N. *Intermolecular and Surface Forces*, 3rd ed.; Elsevier Inc.: Burlington, MA, 2010.

DOI: 10.1021/jacs.6b00179
J. Am. Chem. Soc. 2016, 138, 6765−6773

(2) Klinkova, A.; Therien-Aubin, H.; Choueiri, R. M.; Rubinstein, M.; Kumacheva, E. *Proc. Natl. Acad. Sci. U. S. A.* **2013**, *110* (47), 18775.
(3) Nie, Z.; Fava, D.; Kumacheva, E.; Zou, S.; Walker, G. C.; Rubinstein, M. *Nat. Mater.* **2007**, *6* (8), 609.
(4) Marbella, L. E.; Chevrier, D. M.; Tanchini, P. D.; Shobayo, O.; Smith, A. M.; Johnston, K. A.; Andolina, C. M.; Zhang, P.; Mpourmpakis, G.; Millstone, J. E. *J. Am. Chem. Soc.* **2015**, *137*, 15852.
(5) Dolzhnikov, D. S.; Zhang, H.; Jang, J.; Son, J. S.; Panthani, M. G.; Shibata, T.; Chattopadhyay, S.; Talapin, D. V. *Science* **2015**, *347* (6220), 425.
(6) Peng, X.; Manna, L.; Yang, W.; Wickham, J.; Scher, E.; Kadavanich, A.; Alivisatos, A. *Nature* **2000**, *404* (6773), 59.
(7) Burrows, N. D.; Vartanian, A. M.; Abadeer, N. S.; Grzincic, E. M.; Jacob, L. M.; Lin, W.; Li, J.; Dennison, J. M.; Hinman, J. G.; Murphy, C. J. *J. Phys. Chem. Lett.* **2016**, *7*, 632.
(8) Poirier, G. E.; Pylantt, E. D. *Science* **1996**, *272*, 1145.
(9) Marshall, S. T.; O'Brien, M.; Oetter, B.; Corpuz, A.; Richards, R. M.; Schwartz, D. K.; Medlin, J. W. *Nat. Mater.* **2010**, *9* (10), 853.
(10) Blaser, H. U. *Chem. Rev. (Washington, DC, U. S.)* **1992**, *92* (5), 935.
(11) Rodriguez, J. A.; Hrbek, J. *Acc. Chem. Res.* **1999**, *32* (9), 719.
(12) Cuenya, B. R. *Thin Solid Films* **2010**, *518* (12), 3127.
(13) Skrabalak, S. E.; Au, L.; Li, X.; Xia, Y. *Nat. Protoc.* **2007**, *2* (9), 2182.
(14) Xia, X.; Wang, Y.; Ruditskiy, A.; Xia, Y. *Adv. Mater.* **2013**, *25* (44), 6313.
(15) Sun, Y.; Mayers, B.; Xia, Y. *Adv. Mater.* **2003**, *15* (78), 641.
(16) Macdonald, J. E.; Bar Sadan, M.; Houben, L.; Popov, I.; Banin, U. *Nat. Mater.* **2010**, *9* (10), 810.
(17) Oh, M. H.; Yu, T.; Yu, S.-H.; Lim, B.; Ko, K.-T.; Willinger, M.-G.; Seo, D.-H.; Kim, B. H.; Cho, M. G.; Park, J.-H.; Kang, K.; Sung, Y.-E.; Pinna, N.; Hyeon, T. *Science* **2013**, *340*, 964.
(18) Xiao, F.; Yoo, B.; Lee, K. H.; Myung, N. V. *J. Am. Chem. Soc.* **2007**, *129*, 10068.
(19) Chen, J.; Saeki, F.; Wiley, B. J.; Cang, H.; Cobb, M. J.; Li, Z.; Au, L.; Zhang, H.; Kimmey, M. B.; Li, X.; Xia, Y. *Nano Lett.* **2005**, *5* (3), 473.
(20) Mohl, M.; Kumar, A.; Mohana Reddy, A. L.; Kukovecz, A.; Konya, Z.; Kiricsi, I.; Vajtai, R.; Ajayan, P. M. *J. Phys. Chem. C* **2010**, *114* (1), 389.
(21) Sun, Y.; Xia, Y. *Anal. Chem.* **2002**, *74*, 5297.
(22) Lu, X.; Tuan, H. Y.; Chen, J.; Li, Z. Y.; Korgel, B. A.; Xia, Y. *J. Am. Chem. Soc.* **2007**, *129* (6), 1733.
(23) Smalley, J. F.; Sachs, S. B.; Chidsey, C. E. D.; Dudek, S. P.; Sikes, H. D.; Creager, S. E.; Yu, C. J.; Feldberg, S. W.; Newton, M. D. *J. Am. Chem. Soc.* **2004**, *126* (44), 14620.
(24) Neuhausen, A. B.; Hosseini, A.; Sulpizio, J. a.; Chidsey, C. E. D.; Goldhaber-Gordon, D. *ACS Nano* **2012**, *6* (11), 9920.
(25) Smith, J. G.; Jain, P. K., submitted 2016.
(26) Sönnichsen, C.; Franzl, T.; Wilk, T.; von Plessen, G.; Feldmann, J. *Phys. Rev. Lett.* **2002**, *88* (7), 077402.
(27) Schlather, A. E.; Large, N.; Urban, A. S.; Nordlander, P.; Halas, N. J. *Nano Lett.* **2013**, *13* (7), 3281.
(28) Sherry, L. J.; Jin, R.; Mirkin, C. A.; Schatz, G. C.; Van Duyne, R. P. *Nano Lett.* **2006**, *6* (9), 2060.
(29) Tcherniak, A.; Dominguez-Medina, S.; Chang, W. S.; Swanglap, P.; Slaughter, L. S.; Landes, C. F.; Link, S. *J. Phys. Chem. C* **2011**, *115* (32), 15938.
(30) Sheikholeslami, S.; Jun, Y. W.; Jain, P. K.; Alivisatos, A. P. *Nano Lett.* **2010**, *10* (7), 2655.
(31) Sun, Y.; Mayers, B. T.; Xia, Y. *Nano Lett.* **2002**, *2*, 481.
(32) Andoy, N. M.; Zhou, X.; Choudhary, E.; Shen, H.; Liu, G.; Chen, P. *J. Am. Chem. Soc.* **2013**, *135* (5), 1845.
(33) Han, K. S.; Liu, G.; Zhou, X.; Medina, R. E.; Chen, P. *Nano Lett.* **2012**, *12* (3), 1253.
(34) Ochoa, M. A.; Chen, P.; Loring, R. F. *J. Phys. Chem. C* **2013**, *117* (37), 19074.
(35) Sambur, J. B.; Chen, P. *Annu. Rev. Phys. Chem.* **2014**, *65* (1), 395.
(36) Shen, H.; Zhou, X.; Zou, N.; Chen, P. *J. Phys. Chem. C* **2014**, *118*, 26902.
(37) Xu, W.; Kong, J. S.; Yeh, Y.-T. E.; Chen, P. *Nat. Mater.* **2008**, *7* (12), 992.
(38) Zhou, X.; Choudhary, E.; Andoy, N. M.; Zou, N.; Chen, P. *ACS Catal.* **2013**, *3*, 1448.
(39) Smith, J. G.; Yang, Q.; Jain, P. K. *Angew. Chem., Int. Ed.* **2014**, *53* (11), 2867.
(40) Routzahn, A. L.; Jain, P. K. *Nano Lett.* **2014**, *14* (2), 987.
(41) Routzahn, A. L.; Jain, P. K. *Nano Lett.* **2015**, *15*, 2504.
(42) Ha, J. W.; Ruberu, P. A.; Han, R.; Dong, B.; Vela, J.; Fang, N. *J. Am. Chem. Soc.* **2014**, *136*, 1398.
(43) Wilson, A. J.; Willets, K. A. *Nano Lett.* **2014**, *14* (1), 939.
(44) Thota, S.; Chen, S.; Zhou, Y.; Zhang, Y.; Zou, S.; Zhao, J. *Nanoscale* **2015**, *7* (35), 14652.
(45) Park, Y.; Lee, C.; Ryu, S.; Song, H. *J. Phys. Chem. C* **2015**, *119*, 20125.
(46) Jain, P. K.; Qian, W.; El-Sayed, M. A. *J. Am. Chem. Soc.* **2006**, *128*, 2426.
(47) Pillai, Z. S.; Kamat, P. V. *J. Phys. Chem. B* **2003**, *108* (3), 945.
(48) Zhang, Q.; Li, N.; Goebl, J.; Lu, Z.; Yin, Y. *J. Am. Chem. Soc.* **2011**, *133* (46), 18931.
(49) Smith, J. G.; Faucheaux, J. A.; Jain, P. K. *Nano Today* **2015**, *10* (1), 67.
(50) Alper, J.; Hamad-Schifferli, K. *Langmuir* **2010**, *26* (6), 3786.
(51) Huang, J.; Hemminger, J. C. *J. Am. Chem. Soc.* **1993**, *115*, 3342.
(52) Aldana, J.; Wang, Y. A.; Peng, X. *J. Am. Chem. Soc.* **2001**, *123* (36), 8844.
(53) Aldeek, F.; Hawkins, D.; Palomo, V.; Safi, M.; Palui, G.; Dawson, P. E.; Alabugin, I.; Mattoussi, H. *J. Am. Chem. Soc.* **2015**, *137* (7), 2704.
(54) Chen, J.; Chan, Y. H.; Yang, T.; Wark, S. E.; Son, D. H.; Batteas, J. D. *J. Am. Chem. Soc.* **2009**, *131* (51), 18204.
(55) Hua, B.; Han, K. Y.; Zhou, R.; Kim, H.; Shi, X.; Abeysirigunawardena, S. C.; Jain, A.; Singh, D.; Aggarwal, V.; Woodson, S. a; Ha, T. *Nat. Methods* **2014**, *11* (12), 1233.
(56) Finklea, H.; Hanshew, D. D. *J. Am. Chem. Soc.* **1992**, *114* (9), 3173.
(57) Tarlov, M. J.; Bowden, E. F. *J. Am. Chem. Soc.* **1991**, *113*, 1847.
(58) De Groot, M. T.; Evers, T. H.; Merkx, M.; Koper, M. T. M. *Langmuir* **2007**, *23* (2), 729.
(59) Love, J. C.; Estroff, L. A.; Kriebel J. K.; Nuzzo, R. G.; Whitesides, G. M. *Chem. Rev.* **2005**, *105* (4), 1103.

DOI: 10.1021/jacs.6b00179
J. Am. Chem. Soc. 2016, 138, 6765−6773